Dyes and Pigments 132 (2016) 167–176

Contents lists available at ScienceDirect

Dyes and Pigments

journal homepage: www.elsevier.com/locate/dyepig

Selective "turn-on" probes for CN^- based on a fluorophore skeleton of 1,3-dihydroisobenzofuran

Xue Song Shang, Nian Tai Li, Zhi Qian Guo, Pei Nian Liu*

Shanghai Key Laboratory of Functional Materials Chemistry, Key Lab for Advanced Materials and Institute of Fine Chemicals, East China University of Science and Technology, Meilong Road 130, Shanghai, China

ARTICLE INFO

Article history:
Received 22 March 2016
Received in revised form
29 April 2016
Accepted 30 April 2016
Available online 2 May 2016

Keywords:
1,3-Dihydroisobenzofuran
Cyanide ion
Turn-on
Limit of detection (LOD)
Displacement
Nucleophilic addition

ABSTRACT

Two novel fluorescence "turn-on" cyanide probes based on the 1,3-dihydroisobenzofuran skeleton have been designed and synthesized: a terpyridyl-Cu^{2+} ensemble sensed CN^- in THF-H_2O (1:1, v/v), and a dicyanovinyl-containing compound sensed CN^- in CH_2Cl_2 and THF. Titration of CN^- with terpyridine-Cu^{2+} complex caused a displacement reaction that turned on the fluorescence of **A-Cu^{2+}** at 605 nm. The detection limit of **A-Cu^{2+}** for CN^- was calculated to be 3.15×10^{-6} M. In the presence of CN^-, the dicyanovinyl-bearing probe underwent a nucleophilic addition, showing 85-fold enhancement of fluorescence, with a detection limit of 5.39×10^{-8} M. Our results demonstrate that these two strategies for designing a fluorophore skeleton based on the 1,3-dihydroisobenzofuran lead to highly selective "turn-on" probes for CN^-.

1. Introduction

Cyanide (CN^-) is extremely lethal to mammals because it binds strongly to the active sites of cytochrome *c* oxidase, thereby inhibiting the mitochondrial electron-transport chain, leading to vomiting, convulsions, loss of consciousness and ultimately death [1–5]. The median lethal dose (LD_{50}) of cyanide anion is 0.5–3.5 mg/kg body weight [6–8]. Nevertheless, cyanide is widely used in many industrial processes, such as electroplating, metallurgy, gold mining and chemical processing [9,10]. The seeds of some fruits release cyanide during their intense metabolism. Such environmental exposure poses a threat to health, especially when allowable levels of CN^- in drinking water should not exceed 1.9 μM, according to the World Health Organization [2].

The biological importance and threats of CN^- contamination justify efforts to develop rapid, efficient methods for quantitating the analyte in biological and environmental samples. A variety of conventional methods including electrochemical [11,12], titrimetric [13], atomic absorption spectrometry [14], voltammetric [15] and other techniques [16–19] have been established for the quantitative analysis of CN^-. However, these methods have not been widely applied because they are time-consuming, complex and dependent on expensive instruments. In contrast, fluorescent probes show tremendous promise in this regard, since they are often highly selective and sensitive, simple to use, and inexpensive, and they allow real-time analytes monitoring, not only in chemical and environmental samples but also in living cells via fluorescence confocal microscopy [20–23].

Numerous fluorescent probes have lately been developed in which fluorescence increases in the presence of CN^-. These probes detect CN^- using different mechanisms including hydrogen-bonding interactions [24], metal ion coordination of CN^- [25–31], and deprotonation [32–34]. In 2010 and 2014, Yoon et al. contributed two reviews on various chemosensors for CN^-, in which various "turn-on" mechanisms were discussed in detail [35,36]. One of the most extensively studied mechanisms is nucleophilic addition of CN^- to various fluorophores, including trifluoroacetamide derivatives [37,38], dicyanovinyl [39–42], pyrylium [43], pyridinium [44], indolium [45] and other highly electron-deficient carbonyl groups [46–48].

Recently, we reported the synthesis of a novel 1,3-dihydroisobenzofuran skeleton and its remarkable fluorescence properties [49]. Here we used our previously developed synthetic methods to examine whether 1,3-dihydroisobenzofuran could serve as a fluorophore skeleton to generate probes for CN^- [49–51].

* Corresponding author.
E-mail address: liupn@ecust.edu.cn (P.N. Liu).

http://dx.doi.org/10.1016/j.dyepig.2016.04.051
0143-7208/

Our efforts led to a terpyridine-based "off-on" probe **A-Cu^{2+}** and a dicyanovinyl-based fluorescence-enhancing probe **B** for CN^- (Scheme 1). The terpyridyl-Cu^{2+} complex is non-fluorescent due to the paramagnetic effect that quenches the fluorescence of most probes [52–60]. Once CN^- was added into the above system, fluorescence was restored because of the formation of very stable $[Cu(CN)_x]^{n-}$ species [25–30]. Probe **B** containing a dicyanovinyl group exhibits very weak fluorescence, which is ascribed to the free rotation of the aryl-dicyanovinyl molecular rotor in the excited state, which consumes energy [61,62]. Twisted intramolecular charge transfer (TICT) involving the electron donor in probe **B** quenches the probe's fluorescence in the absence of CN^- [63–66]. Nucleophilic addition of CN^- to the C=C bond of the dicyanovinyl eliminates the intramolecular rotation, greatly intensifying the emission [40].

2. Experimental

2.1. Materials and instruments

4′-(4-Ethynylphenyl)-2,2′:6′,2″-terpyridine (**2**), (*Z*)-(4-(isobenzofuran-1(3*H*)-ylidenemethyl)phenyl)methanol (**5**) and 4-(piperidin-1-yl)benzaldehyde (**6**) were prepared according to the literature methods [67–69]. Bu_4NCN and other chemicals were obtained from commercial sources, and were used without further purification. Tested metal ions Cu^{2+}, Mn^{2+}, Fe^{3+}, Co^{2+}, Ni^{2+}, Zn^{2+}, Hg^{2+}, Mg^{2+}, Ca^{2+} and K^+ were added as chloride salts dissolved in H_2O; other metal ions such as Ag^+, Cd^{2+}, Pb^{2+}, Na^+ were added as nitrate, perchlorate or sulfate salts dissolved in H_2O. Anions such as F^-, Cl^-, Br^-, I^-, AcO^-, $H_2PO_4^-$ were added as tetrabutylammonium salts dissolved in THF or H_2O, SCN^- was added as sodium salt dissolved in EtOH or H_2O and other anions such as S^{2-}, N_3^-, SO_4^{2-}, HCO_3^-, HPO_4^{2-}, PF_6^- were added as sodium, potassium or ammonium salts dissolved in H_2O. Solvents (THF, DMF, DCM) used in the experiments were dried by standard methods prior to use.

^1H NMR and ^{13}C NMR were recorded on a Bruker 400 MHz spectrometer. HRMS were obtained on a Waters LCT Premier XE spectrometer with acetonitrile or methanol as the solvent. The UV absorption spectra were recorded on a Varian Cary 100 spectrophotometer and the fluorescence emission spectra were recorded on a Varian Cary Eclipse fluorescence spectrophotometer. The slit width was 5 nm and PMT voltage was 600 V for both excitation and emission. Chemical shifts (δ, ppm) in the ^1H NMR spectra were recorded using TMS as internal standard. Chemical shifts in $^{13}C\{^1H\}$ NMR spectra were internally referenced to $CHCl_3$ ($\delta = 77.16$ ppm).

2.2. Synthesis of probes *A* and *B*

The synthetic routes of probes **A** and **B** are shown in Scheme 2.

A Sonogashira coupling of (2-iodophenyl)methanol (**1**) and 4′-(4-ethynylphenyl)-2,2′:6′,2″-terpyridine (**2**) in the presence of $PdCl_2(PPh_3)_2$ and CuI afforded the alkynol product **3**. The probe **A** was finally obtained through the tandem reaction of **3** and 4-(dimethylamino)benzaldehyde (**4**) in the presence of *t*-BuOK in THF. Its structure was confirmed by single-crystal X-ray diffraction analysis (Fig. 1).

An addition-elimination of *exo*-cyclic enol ether **5** and 4-(piperidin-1-yl)benzaldehyde (**6**) catalyzed by *t*-BuOK gave the product **7**. Oxidation of **7** using Dess-Martin periodinane generated the aldehyde **8**. A Knoevenagel condensation of **8** and malononitrile afforded the target probe **B**.

2.2.1. Synthesis and characterization of probe *A*

(2-iodophenyl)methanol (**1**) (2.4 mmol, 0.562 g), 4′-(4-ethynylphenyl)-2,2′:6′,2″-terpyridine (**2**) (2.0 mmol, 0.667 g), $PdCl_2(PPh_3)_2$ (0.04 mmol, 28.1 mg) and CuI (0.02 mmol, 3.8 mg) were placed in a 50 mL dry Schlenk flask. Then the flask was evacuated to vacuum and filled with N_2 for three times. Under N_2 atmosphere, DIPA (8.0 mmol, 1.1 mL) and DMF (25 mL) were added and the resulting solution was stirred at 70 °C for 3 h. After the reaction was completed, the mixture was cooled to room temperature and saturated NH_4Cl (aq) was added. The resulting mixture was extracted with EtOAc, and the organic phase was washed with brine and dried over Na_2SO_4. The solvent was evaporated under reduced pressure, and the residue was passed through column chromatography on silica gel (eluent: CH_2Cl_2/MeOH = 50:1, v/v) to afford compound **3** (729.0 mg, 83%).

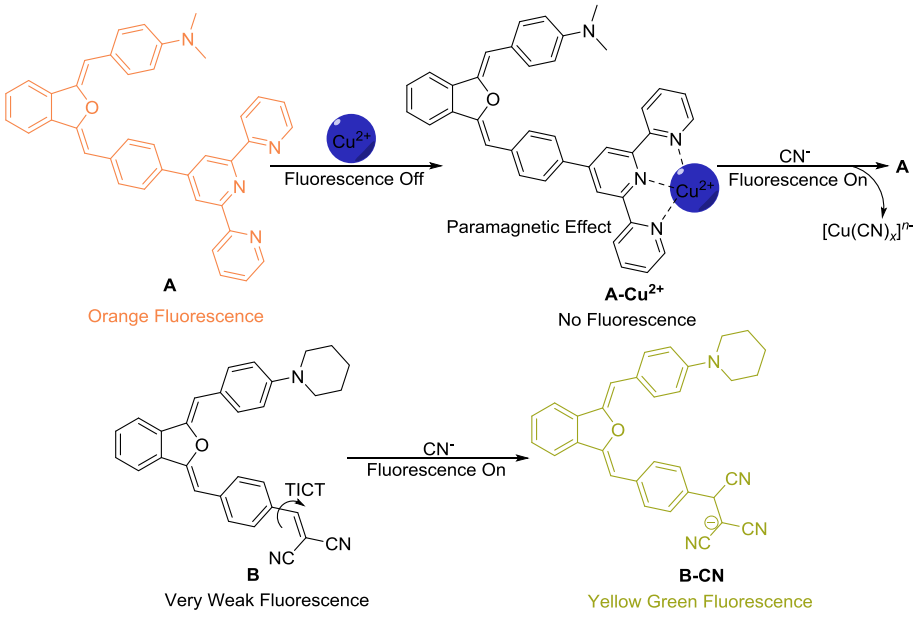

Scheme 1. The structure of probes **A** and **B** and their sensing mechanisms.

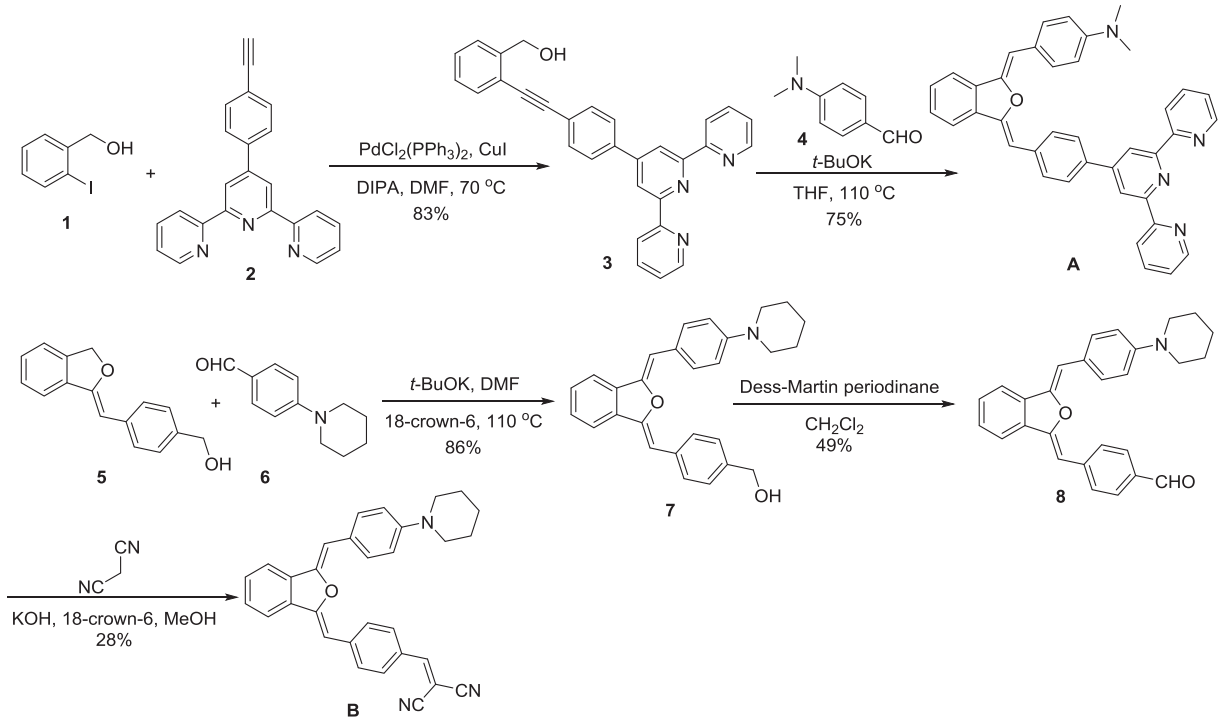

Scheme 2. The synthetic routes of probes **A** and **B**.

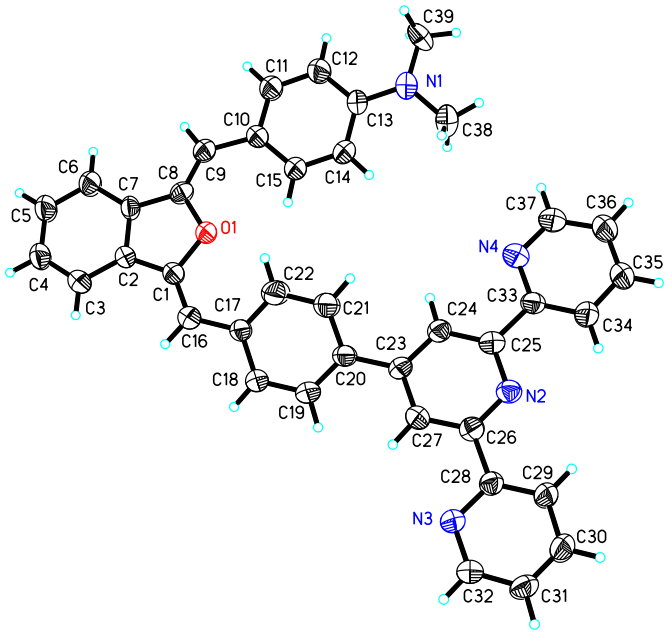

Fig. 1. ORTEP diagram of **A** with ellipsoids drawn at the 30% probability level.

(2-((4-([2,2′:6′,2″-Terpyridin]-4′-yl)phenyl)ethynyl)phenyl) methanol (**3**). ^{1}H NMR (400 MHz, $CDCl_3$, 25 °C) δ 8.73–8.75 (m, 4H), 8.68 (d, J = 7.92 Hz, 2H), 7.87–7.94 (m, 4H), 7.65–7.68 (m, 2H), 7.58 (dd, J_1 = 0.88 Hz, J_2 = 7.48 Hz, 1H), 7.52 (d, J = 7.64 Hz, 1H), 7.35–7.41 (m, 3H), 7.29–7.34 (m, 1H), 4.97 (d, J = 5.92 Hz, 2H), 2.24 (br s, 1H); ^{13}C NMR (100.6 MHz, $CDCl_3$, 25 °C) δ 156.22, 156.14, 149.39, 149.26, 142.81, 138.48, 137.08, 132.36, 132.21, 129.02, 127.57, 127.44, 127.33, 124.07, 123.80, 121.55, 121.21, 118.77, 93.97, 88.34, 63.99; HRMS (ESI, TOF) calcd for $C_{30}H_{22}N_3O^+$ $[M + H]^+$: 440.1757, found: 440.1753.

To a mixture of **3** (0.5 mmol, 219.8 mg) and 4-(dimethylamino) benzaldehyde (**4**) (0.75 mmol, 111.9 mg) in THF (5.0 mL) at room temperature was added *t*-BuOK (0.6 mmol, 1 M in THF) via a syringe. The reaction mixture was then heated to 110 °C in a sealed tube under nitrogen atmosphere and stirred for 4 h. After the mixture was cooled to ambient temperature, it was diluted with saturated NH_4Cl (aq) and extracted with EtOAc. The organic phase was washed with brine and dried over Na_2SO_4. The solvent was evaporated under reduced pressure, and the residue was passed through column chromatography on silica gel (eluent: CH_2Cl_2/MeOH = 80:1, v/v) to afford the target probe **A** as an orange solid (214.0 mg, 75%).

4-(((*Z*)-3-((*Z*)-4-([2,2′:6′,2″-Terpyridin]-4′-yl)benzylidene)isobenzofuran-1(3*H*)-ylidene)methyl)-*N*,*N*-dimethylaniline (**A**). Mp: 218.6–222.2 °C; ^{1}H NMR (400 MHz, $CDCl_3$, 25 °C) δ 8.80 (s, 2H), 8.75–8.77 (m, 2H), 8.70 (d, J = 7.96 Hz, 2H), 7.99–8.07 (m, 4H), 7.90 (td, J_1 = 1.80 Hz, J_2 = 7.68 Hz, 2H), 7.84 (d, J = 8.84 Hz, 2H), 7.62–7.69 (m, 2H), 7.35–7.43 (m, 4H), 6.87 (d, J = 8.84 Hz, 2H), 6.22 (s, 1H), 6.19 (s, 1H), 3.07 (s, 6H); ^{13}C NMR (100.6 MHz, CDCl3, 25 °C) δ 156.54, 156.02, 153.06, 150.24, 149.50, 149.25, 149.15, 137.04, 136.55, 135.79, 134.67, 133.26, 129.83, 129.37, 128.76, 128.43, 127.62, 123.94, 123.25, 121.59, 120.02, 119.41, 118.71, 112.74, 101.12, 98.09, 40.74; HRMS (EI, TOF) calcd for $C_{39}H_{30}N_4O$ $[M]^+$: 570.2420, found: 570.2419.

2.2.2. Synthesis and characterization of probe *B*

(*Z*)-(4-(isobenzofuran-1(3*H*)-ylidenemethyl)phenyl)methanol (**5**) (190.6 mg, 0.8 mmol), 4-(piperidin-1-yl)benzaldehyde (**6**) (227.2 mg, 1.2 mmol), *t*-BuOK (0.48 mmol, 1 M in THF) and 18-crown-6 (190.4 mg, 0.72 mmol) in DMF (4 mL) were stirred at 110 °C under nitrogen atmosphere for 3 h. The mixture was cooled and saturated NH_4Cl (aq) was added to quench the reaction. The resulting mixture was extracted with CH_2Cl_2 and the organic phase was washed with brine, dried over Na_2SO_4. The solvent was evaporated and the residue was passed through column

chromatography on silica gel (eluent: PE/EtOAc = 10:1, v/v) to afford the crude product (4-((*Z*)-((*Z*)-3-(4-(piperidin-1-yl)benzylidene)isobenzofuran-1(3*H*)-ylidene)-methyl)phenyl)methanol **7** (282.0 mg, 86%) without further purification [49].

Dess-Martin periodinane (350.5 mg, 0.83 mmol) was added to a stirred solution of **7** (282.0 mg, 0.69 mmol) in DCM (40 mL). The solution was stirred at room temperature for 1 h and diluted with 10 mL of DCM. Saturated aqueous $NaHCO_3$ and 3 M aqueous $Na_2S_2O_3$ were added to quench the reaction [70]. The organic layer was separated and washed with brine, dried over Na_2SO_4. After the solvent was evaporated, the residue was passed through flash column chromatography on silica gel (eluent: PE/EtOAc = 60:1, v/v) to give the oxidation product 4-((*Z*)-((*Z*)-3-(4-(piperidin-1-yl)benzylidene)isobenzofuran-1(3*H*)-ylidene)methyl)benzaldehyde **8** (138.6 mg, 49%) for the next reaction.

Malononitrile (29.1 mg, 0.44 mmol), KOH (5.7 mg, 0.10 mmol) and 18-crown-6 (27.0 mg, 0.10 mmol) were successively added to a stirred solution of **8** (138.6 mg, 0.34 mmol) in MeOH (30 mL). The solution was stirred at room temperature for 1 h and 30 mL water was added. The resulting mixture was exacted with DCM and the organic phase was washed with brine, dried over Na_2SO_4. The solvent was evaporated under reduced pressure, and the residue was passed through column chromatography on silica gel (eluent: PE/EtOAc = 40:1, v/v) to afford the final probe **B** as a brownish black solid (43.3 mg, 28%) [71].

2-(4-((*Z*)-((*Z*)-3-(4-(Piperidin-1-yl)benzylidene)isobenzofuran-1(3*H*)-ylidene)methyl)benzylidene)malononitrile (**B**). Mp: 207.6–210.8 °C; ^{1}H NMR (400 MHz, $CDCl_3$, 25 °C) δ 7.99 (d, J = 8.52 Hz, 2H), 7.94 (d, J = 8.52 Hz, 2H), 7.77 (d, J = 8.64 Hz, 2H), 7.64–7.69 (m, 3H), 7.40–7.50 (m, 2H), 7.00 (d, J = 8.32 Hz, 2H), 6.26 (s, 1H), 6.18 (s, 1H), 3.30 (t, J = 5.04 Hz, 4H), 1.74 (br s, 4H), 1.63–1.65 (m, 2H); ^{13}C NMR (100.6 MHz, $CDCl_3$, 25 °C) δ 158.68, 155.92, 151.05, 149.25, 142.75, 134.91, 132.55, 131.48, 130.45, 130.00, 128.88, 128.66, 128.29, 120.55, 119.67, 115.74, 114.76, 113.60, 102.73, 97.62, 79.40, 49.90, 25.77, 24.47; HRMS (EI, TOF) calcd for $C_{31}H_{25}N_3O$ $[M]^+$: 455.1998, found: 455.1999.

3. Results and discussion

3.1. Spectral characteristics of probe *A*

Since probe **A** is hydrophobic, we used THF-H_2O (1:1, v/v) as the solvent in which to analyze its ability to detect Cu^{2+}. The emission intensity of **A** showed a linear dependence on Cu^{2+} concentration, and the probe showed high selectivity and sensitivity.

The UV–vis absorption spectra of probe **A** show a slightly lower and red-shifted absorption inflection point in THF-H_2O (1:1, v/v) than in THF (Fig. S1a, Supporting Information). The emission peak of **A** is bathochromic-shifted and less than half as intense in THF-H_2O as in THF (Fig. S1b, Supporting Information). These results show that water significantly affects the photophysical properties of probe **A**.

Next we explored how the fluorescence spectra of **A** vary with solvent polarity. Since **A** is a probe with push–pull effect in which

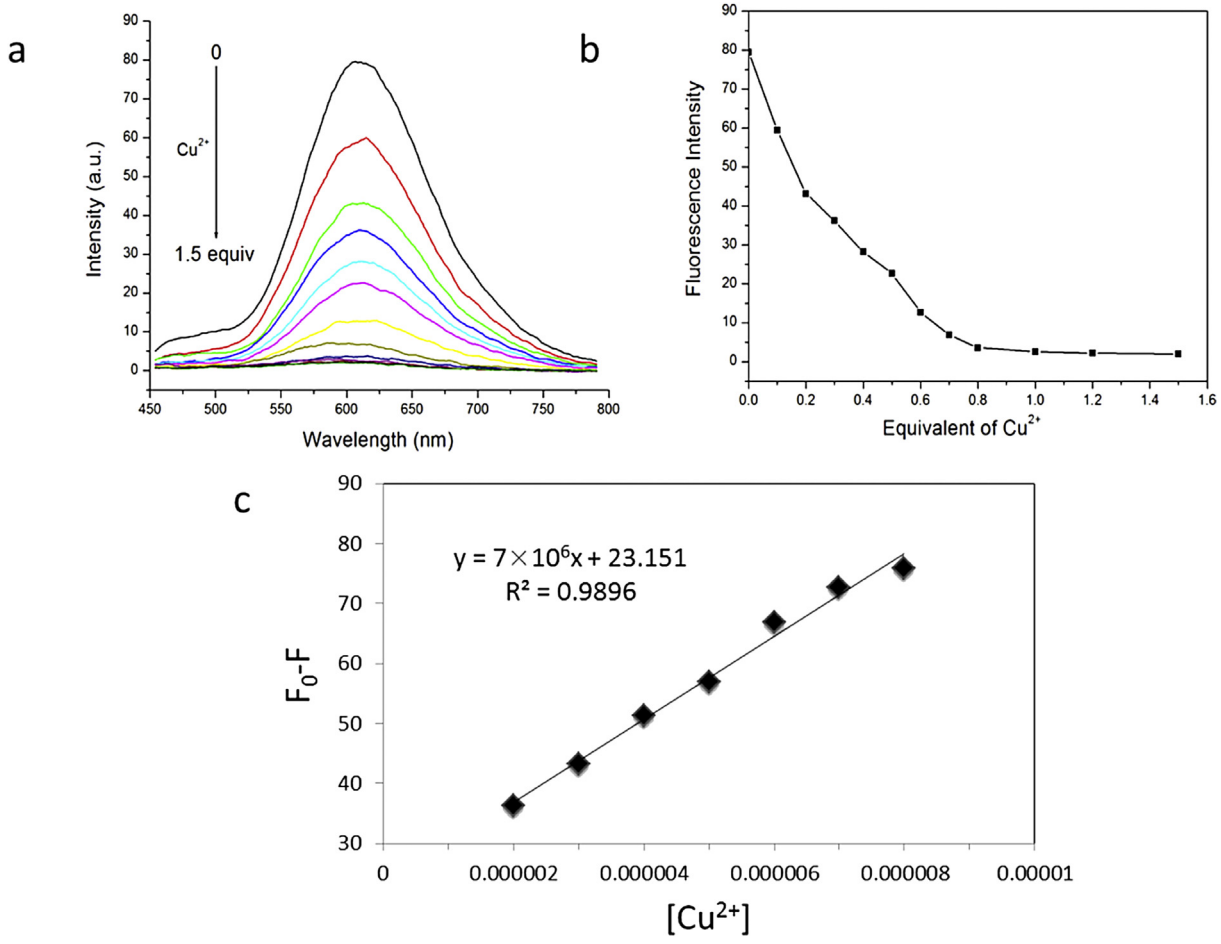

Fig. 2. (a) Fluorescence titration spectra of **A** (10 μM) upon addition of Cu^{2+} (0–1.5 equiv.) in THF-H_2O (1:1, v/v) at 25 °C. (b) Variations in fluorescence intensity of probe **A** (10 μM) at 611 nm as a function of Cu^{2+} equivalents. (c) Linear Job's plot of F_0–F at 611 nm as a function of Cu^{2+} concentration. F_0 is the fluorescence intensity of **A** in the absence of any metal ion. Excitation wavelength: 435 nm.

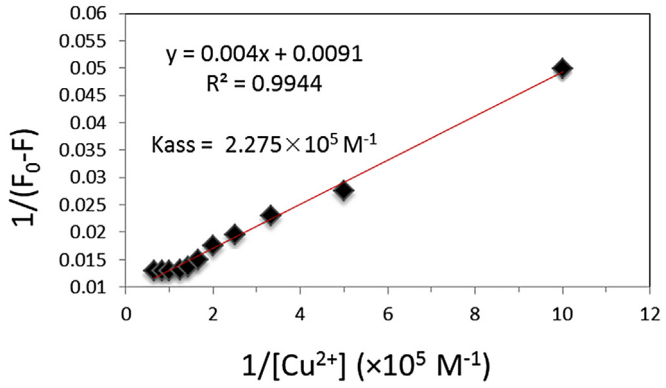

Fig. 3. Benesi–Hildebrand linear analysis plot of **A** at different Cu^{2+} concentrations.

N,*N*-dimethylamine serves as the electron-donor and terpyridyl serves as the electron-acceptor, it is strongly affected by solvent polarity. The absorption spectra of **A** was similar in various solvents, while the emission spectra varied substantially (Fig. S2a-b). The maximal emission wavelength red-shifted with the increasing solvent polarity (from toluene to DMSO): the emission peak was red-shifted by 82 nm in DMSO relative to its position in toluene. The effect of solvent polarity was further confirmed by comparison of normalized fluorescence spectra of **A** in different solvents, which can provide a more intuitive illustration of solvent effect on the emission peak (Fig. S2c, Supporting Information). Fluorescence photographs of **A** in different solvents show the color change from cyan to magenta with the increasing solvent polarity (Fig. S2d).

We also investigated the effect of pH values on the fluorescence emission of probe **A** in THF-H_2O (1:1, v/v) (Fig. S3). As shown in Fig. S3, the probe **A** was almost non-fluorescent when the pH value of solution is 1 due to the protonation of terpyridyl group to form terpyridinium ion, thus exhibiting a stronger ICT effect in the excited state [72]. The fluorescence intensity of **A** increased notably when the pH value of solution enhanced to 2–4. In the pH value region of 5–14, the fluorescence spectra of **A** exhibited no obvious difference, indicating that **A** was not protonated under the conditions of weak acidity.

To test the selectivity of probe **A** for Cu^{2+} over other metal ions, we mixed **A** (10 μM) with 10 equivalents of metal ions in THF-H_2O (1:1, v/v). The absorption inflection point of **A** increased in absorbance when $CoCl_2$ was added, while the absorption inflection point at 435 nm disappeared when $CuCl_2$ was added (Fig. S4a, Supporting Information). Among the metal ions tested, only Cu^{2+} significantly quenched the fluorescence emission of **A** (Fig. S4b, Supporting Information). The bar graph (Fig. S4c, Supporting Information) as well as the changes in color and fluorescence of **A** in THF-H_2O (Fig. S4d, Supporting Information) further confirmed the high selectivity of **A** for Cu^{2+}.

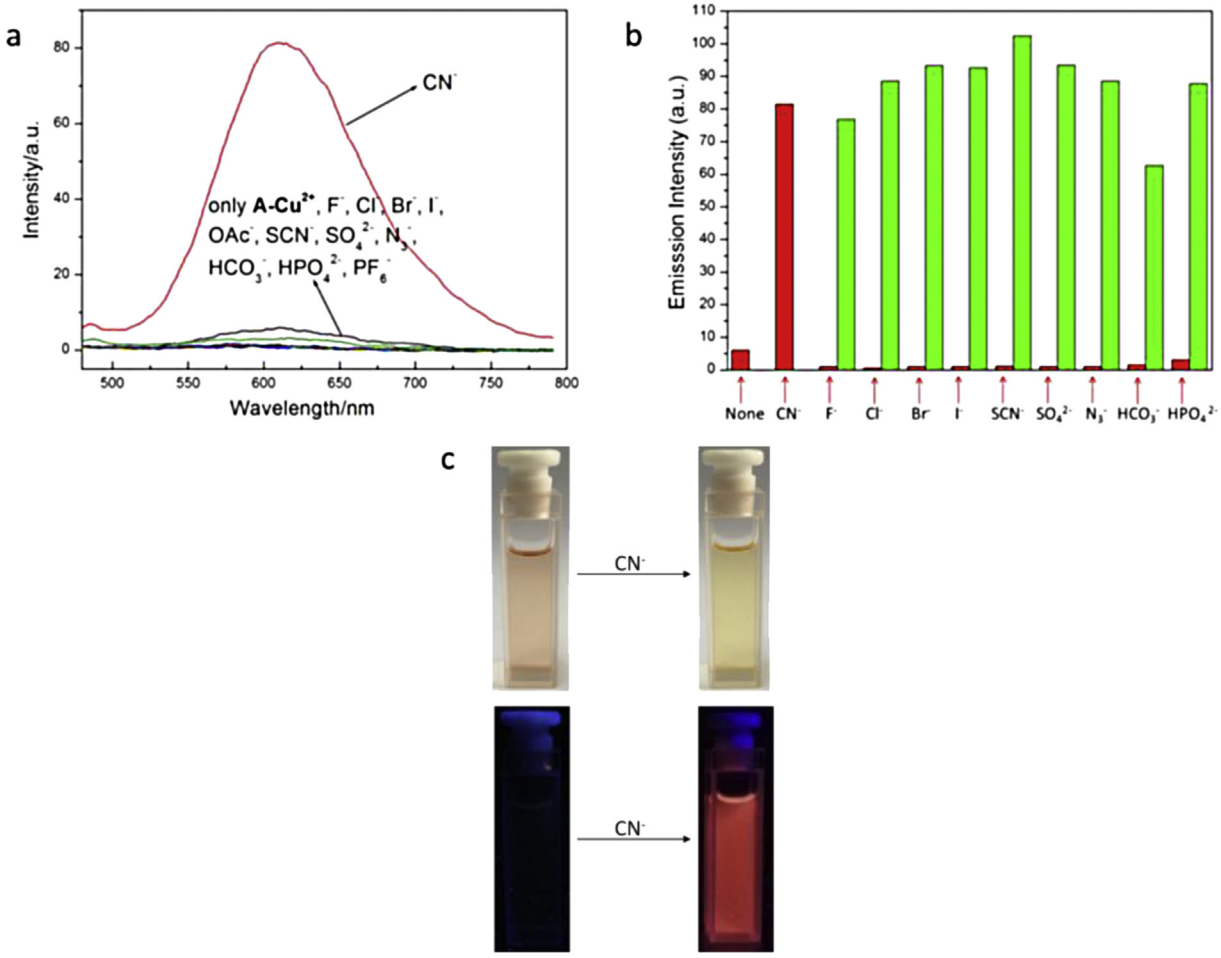

Fig. 4. (a) Changes in the emission spectrum of **A-Cu^{2+}** (10 μM) in the presence of different aqueous anions (CN^-, 50 equiv.; others, 100 equiv.) in THF-H_2O (1:1, v/v) at 25 °C. (b) The bar graph of fluorescence intensity at 611 nm in the presence of various anions. Red bars indicate fluorescence intensity in the absence of any anion or in the presence of the indicated anion (CN^-, 50 equiv.; others, 100 equiv.). Green bars indicate fluorescence intensity in the presence of both CN^- (50 equiv.) and the indicated anion (100 equiv.). (c) Changes in **A-Cu^{2+}** color (above) and fluorescence (below) in THF-H_2O (1:1, v/v) upon addition of CN^-. The fluorescence photograph was taken under 365 nm UV light. Excitation wavelength: 435 nm. (For interpretation of the references to color in this figure legend, the reader is referred to the web version of this article.)

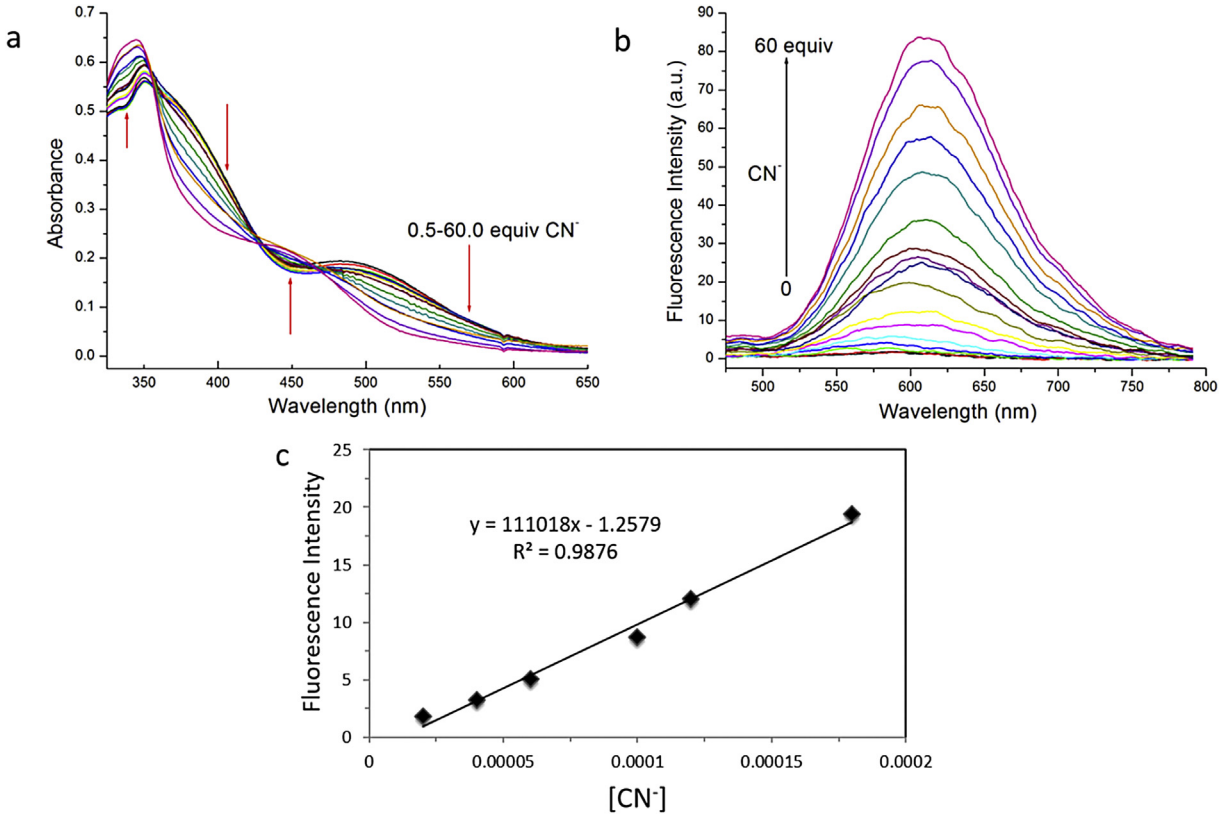

Fig. 5. UV absorption (a) and fluorescence (b) titration spectra of **A-Cu**$^{2+}$ (10 μM) in THF-H_2O (1:1, v/v) at 25 °C in the presence of 0–60.0 equiv. CN^-. (c) The linear Job's plot of fluorescence intensity at 605 nm as a function of concentration of CN^-. Excitation wavelength: 435 nm.

The maximum emission peak of **A** in the absence of Cu^{2+} emerged at 611 nm (Fig. 2a). The fluorescence intensity gradually decreased with the addition of Cu^{2+} from 0 to 1.5 equiv. The fluorescence intensity reached a plateau at concentrations of Cu^{2+} beyond 10 μM (Fig. 2b). The limit of detection (LOD) for Cu^{2+} was calculated to be 1.13 × 10^{-7} M based on analysis of 10 blank solutions and the IUPAC definition of LOD as 3σ/k, where σ is the standard deviation and k is the slope of the linear Job's plot [73] (Fig. 2c).

A Job's plot of the relationship between $(F_0-F)/F_0$ and $[Cu^{2+}]/\{[Cu^{2+}]+[\mathbf{A}]\}$ (Fig. S5a, Supporting Information) showed that $(F_0-F)/F_0$ reached a plateau when $[Cu^{2+}]/\{[Cu^{2+}]+[\mathbf{A}]\}$ was 0.5. This

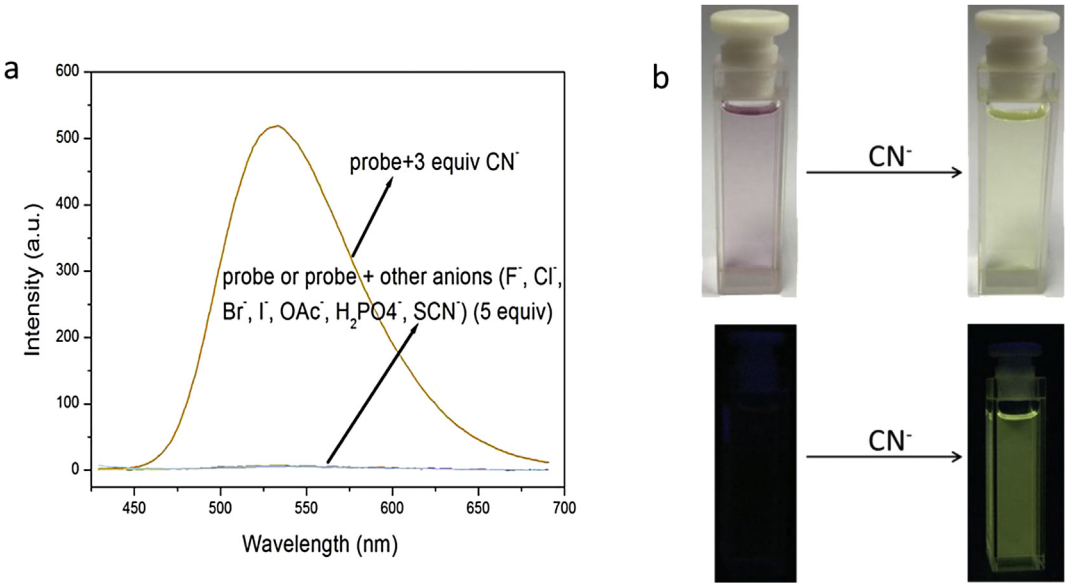

Fig. 6. (a) Fluorescence spectra of **B** (10 μM) in CH_2Cl_2 at 25 °C in the absence or presence of CN^- (3 equiv.) or other anions (5 equiv.). Excitation wavelength: 410 nm. (b) Changes in color (above) and fluorescence (below) of **B** in CH_2Cl_2 after the addition of CN^-. The fluorescence photograph was taken under 365 nm UV light.

confirms 1:1 stoichiometry between **A** and Cu^{2+}. In addition, HRMS indicated a mass of 633.1710 for [**A** + Cu^{2+}], which matches the calculated mass of 633.1717 for $C_{39}H_{30}ON_4Cu$ (Fig. S5b, Supporting Information). A Benesi-Hildebrand plot obtained from the fluorescence titration data afforded an association constant of 2.275×10^5 M^{-1} [74] (Fig. 3).

Finally, we investigated the fluorescence responses of probe **A** to $CuCl_2$, $CuSO_4$ and $Cu(NO_3)_2$ in THF/H_2O (1:1, v/v) in order to investigate the influence of anionic counter ions (Fig. S6, Supporting Information). The result showed that $CuCl_2$ and $CuSO_4$ quenched the fluorescence of **A** with slightly higher efficiency than $Cu(NO_3)_2$. The reason is possibly that **A** coordinates with $Cu(NO_3)_2$ more weakly than with $CuCl_2$ or $CuSO_4$.

3.2. Spectral characteristics of probe ***A-Cu*$^{2+}$ for CN^- detection

Considering the non-fluorescence of the terpyridyl-Cu^{2+} ensemble and the strong affinity of CN^- with Cu^{2+}, we used **A-Cu**$^{2+}$ complex to detect CN^- in THF-H_2O (1:1, v/v). The selectivity of **A-Cu**$^{2+}$ for CN^- over other anions was investigated by adding 50 equiv. of CN^- or 100 equiv. of other anions to **A-Cu**$^{2+}$ (10 μM) in THF-H_2O (1:1, v/v). Only CN^- significantly increased the fluorescence at 611 nm by more than 12-fold, and the fluorescence quantum yield (Φ_F) increased from 0.02% to 0.65%. Whereas, other anions such as F^-, Cl^-, Br^-, I^-, OAc^-, SCN^-, SO_4^{2-}, N_3^-, HCO_3^-, HPO_4^{2-} and PF_6^- induced almost no change in fluorescence (Fig. 4a). The bar graph (Fig. 4b) as well as the changes in color and fluorescence of **A-Cu**$^{2+}$ in THF-H_2O (Fig. 4c) further confirmed the high selectivity of **A-Cu**$^{2+}$ for CN^-.

UV absorption and fluorescence titration experiments were performed to analyze the response of **A-Cu**$^{2+}$ in THF-H_2O (1:1, v/v) to the addition of CN^-. The UV absorption titration spectrum of **A-Cu**$^{2+}$ with CN^- in THF-H_2O showed three isosbestic points at approximately 356, 428 and 466 nm. The absorption inflection point at about 482 nm gradually disappeared with the addition of CN^- and a new inflection point emerged at about 450 nm when 60 equiv. of CN^- was added (Fig. 5a). The fluorescence titration spectrum of **A-Cu**$^{2+}$ with CN^- showed a peak of maximum emission at 605 nm, and the fluorescence intensity gradually increased with increasing amount of CN^- from 0 to 60.0 equiv. (Fig. 5b). The detection limit of **A-Cu**$^{2+}$ for CN^- in THF-H_2O (1:1, v/v) was measured to be 3.15×10^{-6} M based on analysis of 10 blank solutions and the linear Job's plot (Fig. 5c).

3.3. Spectral characteristics of probe ***B*** for CN^- detection

The selectivity of probe **B** for CN^- over other anions was investigated by adding 3 equiv. of CN^- or 5 equiv. of other anions to **B** (10 μM) in CH_2Cl_2. Only CN^- substantially increased the fluorescence of **B** (Φ_F changed from 0.072% to 4.5%), with the other anions barely affecting the emission (Fig. 6a). The selectivity for CN^- was further confirmed based on analysis of the visible color change and the fluorescence enhancement upon addition of CN^- (Fig. 6b).

The UV absorption titration spectrum of **B** with CN^- in CH_2Cl_2 showed three isosbestic points at approximately 338, 410 and 455 nm. Upon addition of CN^-, the absorbance of **B** in CH_2Cl_2 at 378 nm gradually decreased and the absorption peak red-shifted.

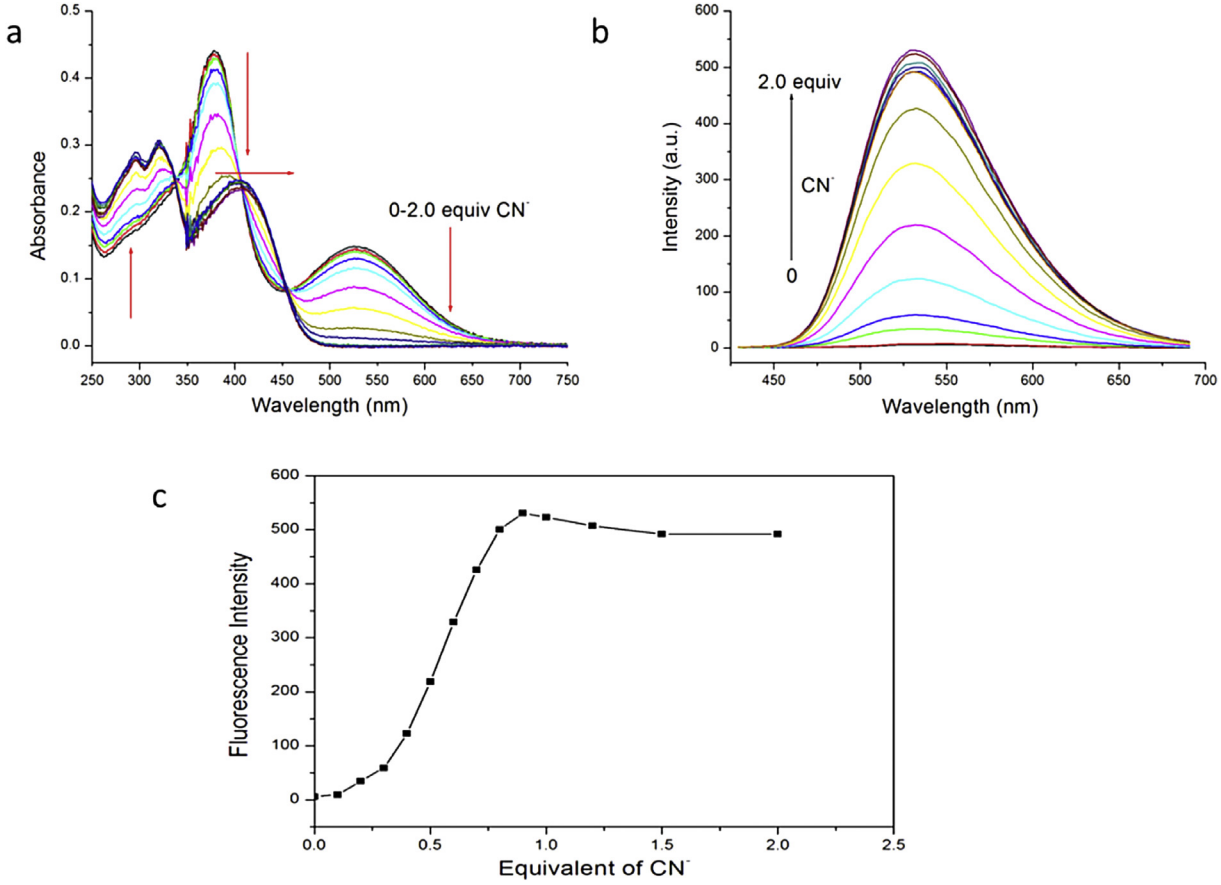

Fig. 7. UV absorption (a) and fluorescence (b) titration spectra of **B** (10 μM) in CH_2Cl_2 at 25 °C in the presence of 0–2.0 equiv. CN^-. (c) Variation of the fluorescence intensity of probe **B** (10 μM) at 531 nm in the presence of increasing amounts of CN^-. Excitation wavelength: 410 nm.

The absorption peak at 525 nm gradually disappeared with increasing concentration of CN^- (Fig. 7a). The fluorescence titration spectrum of **B** with CN^- showed a peak of maximum emission at 531 nm, and the fluorescence intensity gradually increased with increasing CN^- from 0 to 2.0 equiv. (Fig. 7b). The fluorescence intensity reached a plateau at a CN^- concentration of 9 μM (Fig. 7c).

To measure the real-time sensitivity of probe **B** toward CN^- in CH_2Cl_2, we measured the fluorescence intensity every 15 s after addition of 1.5 equiv. of CN^- (Fig. S7a, Supporting Information). The fluorescence intensity increased rapidly to 111 a.u. within 15 s, and it reached a plateau after approximately 1 min (Fig. S7b, Supporting Information). These results indicate that probe **B** responds rapidly to CN^-. Assuming a first-order reaction between **B** and CN^- in the interval from 30 to 240 s, we determined an apparent rate constant of 0.0086 s^{-1} (Fig. S7c, Supporting Information).

Subsequently, we investigated how different aqueous anions affect the photophysical properties of **B** in THF. As shown in Fig. S8a, CN^- enhanced the emission of **B** at 528 nm more than 15-fold (Φ_F changed from 0.076% to 0.84%), while F^- enhanced the emission at 546 nm only 4-fold and I^- enhanced it at 542 nm only 3.7-fold. The fluorescence intensity changed negligibly in the presence of other aqueous anions. The high selectivity of **B** for CN^- in THF was confirmed based on analysis of the visible color change and the fluorescence enhancement upon addition of CN^- (Fig. S8b), as well as based on comparison of the fluorescence enhancement in the presence of various anions (Fig. S8c).

The UV absorption and fluorescence titration experiments were performed to analyze the response of **B** in THF to the addition of aqueous CN^-. As CN^- concentration increased, the absorbance at 374 nm gradually decreased concomitantly with red-shifting of the absorption peak. At the same time, the absorption peak at 516 nm gradually disappeared (Fig. S9a, Supporting Information). The fluorescence titration spectra of **B** with aqueous CN^- showed a peak of maximum emission at 533 nm (Fig. S9b, Supporting Information). The fluorescence intensity increased rapidly in the presence of 0–1.0 equiv. CN^-, then more slowly with further addition of aqueous CN^- (Fig. S9c, Supporting Information). The fluorescence intensity varied linearly with the concentration of CN^- in the range of 0.1–0.8 equiv. (Fig. S9d, Supporting Information). Using the same IUPAC definition of LOD as for probe **A**, we calculated an LOD of 5.39×10^{-8} M for probe **B** and CN^-, based on the linear Job's plot and 10 blank solutions.

Finally, we investigated the real-time fluorescence response of **B** (10 μM) in THF upon addition of 2.5 equiv. of CN^- (Fig. 8a). The fluorescence intensity at 532 nm increased approximately 14-fold in the first 30 s, after which it increased slowly but steadily beyond 60 s (Fig. 8b). The results indicate that **B** is highly sensitive to CN^-. Assuming a pseudo-first-order reaction between **B** and CN^- in THF during the interval from 1 to 15 min, we determined the apparent rate constant to be 0.0545 min^{-1} (Fig. 8c).

To better understand the interaction between **B** and CN^-, we isolated and characterized the addition product (Fig. S10, Supporting Information). By ^1H NMR, addition of CN^- to **B** caused the dicyanovinylic proton signal at 7.69 ppm to disappear and two doublet peaks to emerge at 4.50 and 4.27 ppm. By ^{13}C NMR, addition of CN^- eliminated the signal of the dicyanovinylic carbon close

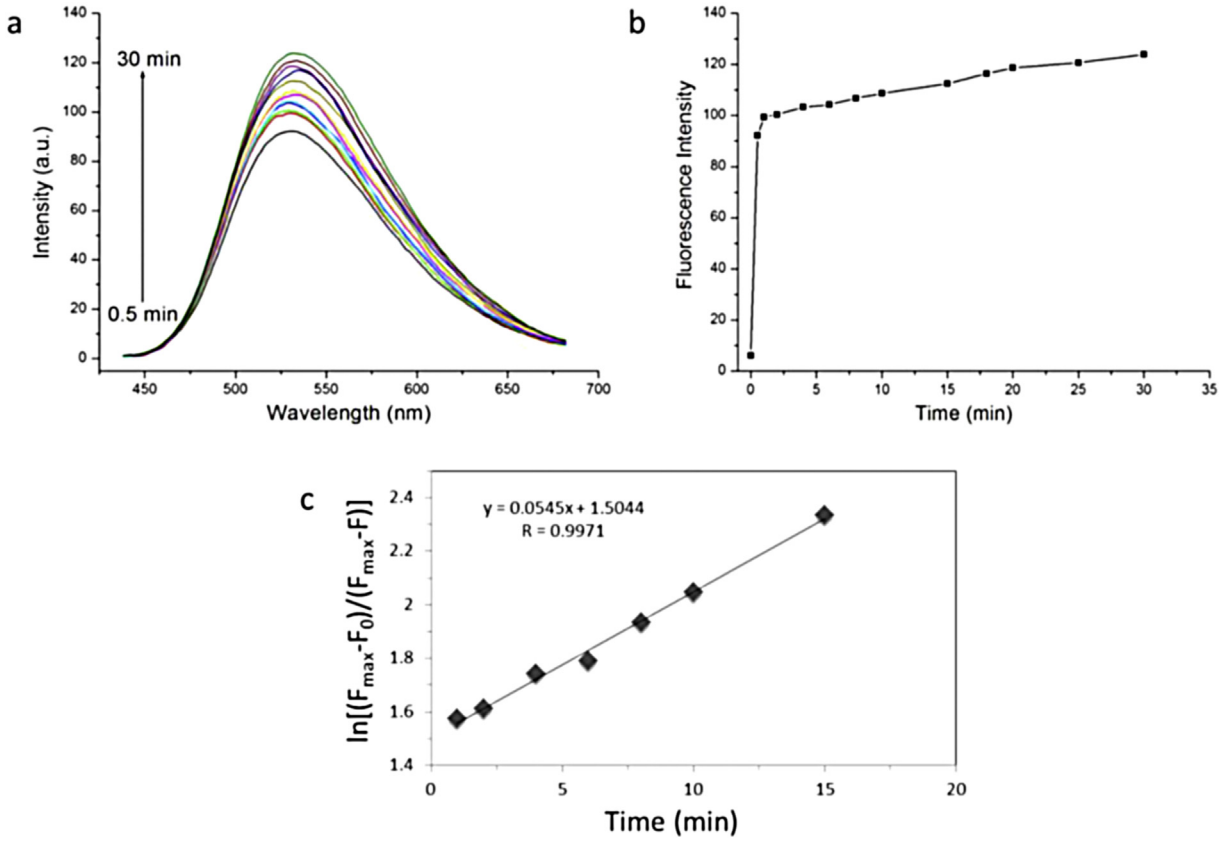

Fig. 8. (a) Fluorescence intensity of probe **B** (10 μM) in THF at 25 °C upon addition of 2.5 equiv. of aqueous CN^-. The indicated curves were obtained at 0.5, 1, 2, 4, 6, 8, 10, 15, 18, 20, 25 and 30 min. (b) Time course of the fluorescence response of **B** (10 μM) in THF upon addition of 2.5 equiv. of aqueous CN^-. (c) Kinetic analysis of the reaction between **B** and CN^- in THF during the interval from 1 to 15 min according to a pseudo-first-order model. F_{max}: The maximum fluorescence intensity of probe **B** within 30 min after addition of 2.5 equiv. of aqueous CN^-. F_0: The fluorescence intensity of **B** in THF in the absence of CN^-. Excitation wavelength: 410 nm.

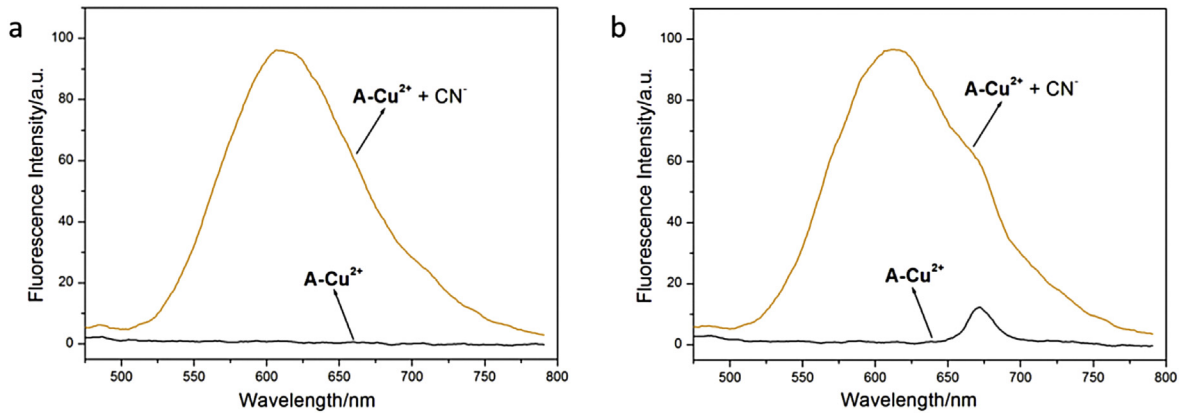

Fig. 9. Fluorescence spectra of probe **A-Cu^{2+}** (10 μM) in THF-tap water (1:1, v/v) (a) or THF-river water (1:1, v/v) (b) at 25 °C before and after the addition of 50 equiv. of aqueous CN^-. Excitation wavelength: 435 nm.

to the cyano group at 79.40 ppm, and caused two peaks to emerge at 39.06 and 29.87 ppm. In addition, HRMS in ESI mode showed a mass peak at 483.2182 for [**B**–CN + H], consistent with the calculated mass of 483.2185 for $C_{32}H_{27}N_4O$ ($[M + H]^+$). These results are in accordance with a nucleophilic addition mechanism (Scheme 1).

3.4. Real sample analysis

For the real sample analysis, we used probes **A-Cu^{2+}** and **B** to detect CN^- in tap water or river water obtained from Qingchun River in our campus. The probe **A-Cu^{2+}** was non-fluorescent in THF-tap water (1:1, v/v) or THF-river water (1:1, v/v). Once 50 equiv. of CN^- in tap water or river water were added, the fluorescence intensity increased significantly (Fig. 9). The result was consistent with that obtained in THF-H_2O (1:1, v/v). For probe **B**, we also observed the fluorescence enhancement when 5 equiv. of CN^- dissolved in tap water or river water were added (Fig. S11), which was consistent with the result using deionized water. These results proved the potential of these two probes in practical applications for the real samples.

4. Conclusions

In summary, we have developed two novel fluorescence "turn-on" cyanide probes based on a new 1,3-dihydroisobenzofuran skeleton. One is the complex **A-Cu^{2+}**, which is non-fluorescent due to the paramagnetic effect of Cu^{2+}. However, it is selective for CN^- via a displacement mechanism with an LOD of 3.15×10^{-6} M in THF-H_2O (1:1, v/v). The other is a dicyanovinyl-based probe **B,** which emits very weak fluorescence due to TICT in the excited state. Nucleophilic addition of CN^- to the dicyanovinyl group eliminates the intramolecular free rotation, enhancing the fluorescence. The LOD of **B** for CN^- is 5.39×10^{-8} M in THF, which lies well below the WHO-defined limit of 1.9 μM for CN^- in drinking water. Based on these results, we draw the conclusion that probe **B** is much more sensitive for CN^- than probe **A-Cu^{2+}**. The real sample analysis of CN^- in tap water and river water using both probes proves their potential usage in practical applications of environmental field.

Acknowledgments

This work was supported by the National Natural Science Foundation of China (Project Nos. Project Nos. 21421004, 21190033, 21372072 and 21561162003), NCET (NCET-13-0798), the Basic Research Program of the Shanghai Committee of Sci. & Tech. (Project No. 13M1400802), the Program for Eastern Scholar Distinguished Professor and the Fundamental Research Funds for the Central Universities.

Appendix A. Supplementary data

Supplementary data related to this article can be found at http://dx.doi.org/10.1016/j.dyepig.2016.04.051.

References

[1] Vennesland B, Comm EE, Knownles CJ, Westly J, Wissing F. Cyanide in biology. London: Academic Press; 1981.
[2] Baird C, Cann M. Environmental chemistry. New York: Freeman; 2005.
[3] Peng MJ, Guo Y, Yang XF, Wang LY, An J. A highly selective ratiometric and colorimetric chemosensor for cyanide detection. Dyes Pigments 2013;98:327–32.
[4] Steed JW. A modular approach to anion binding podands: adaptability in design and synthesis leads to adaptability in properties. Chem Commun 2006:2637–49.
[5] Yang Y, Yin C, Huo F, Chao J, Zhang Y, Cheng F. A new highly selective and turn-on fluorescence probe for detection of cyanide. Sens Actuators B 2014;193:220–4.
[6] Tomasulo M, Sortino S, White AJP, Raymo FM. Chromogenic oxazines for cyanide detection. J Org Chem 2006;71:744–53.
[7] Koenig R. Wildlife deaths are a grim wake-up call in Eastern Europe. Science 2000;287:1737–8.
[8] Muir GD. Hazards in the chemical laboratory. London: The Royal Chemical Society; 1977.
[9] Miller GC, Pritsos CA. Cyanide Soc Ind Econ Aspects Proc Symp Annu Meet TMS 2001:73–81.
[10] Kulig K. Cyanide toxicity. Atlanta, GA: U. S. Department of Health and Human Services; 1991.
[11] Timofeyenko YG, Rosentreter JJ, Mayo S. Piezoelectric quartz crystal microbalance sensor for trace aqueous cyanide ion determination. Anal Chem 2007;79:251–5.
[12] Abbaspour A, Asadi M, Ghaffarinejad A, Safaei E. A selective modified carbon paste electrode for determination of cyanide using tetra-3,4-pyridinoporphyrazinatocobalt(II). Talanta 2005;66:931–6.
[13] Anzenbacher PJ, Tyson DS, Jursikova K, Castellano FN. Luminescence lifetime-based sensor for cyanide and related anions. J Am Chem Soc 2002;124:6232–3.
[14] Noroozifar M, Khorasani-Motlagh M, Hosseini SN. Flow injection analysis–-flame atomic absorption spectrometry system for indirect determination of cyanide using cadmium carbonate as a new solid-phase reactor. Anal Chim Acta 2005;528:269–73.
[15] Suzuki T, Hiolki A, Kurahashi M. Development of a method for estimating an accurate equivalence point in nickel titration of cyanide ions. Anal Chim Acta 2003;476:159–65.
[16] Lebeda FJ, Deshpande SS. Potentiometric measurements of hydrogen and cyanide ions in buffered media. Anal Biochem 1990;187:302–9.
[17] Dadfarnia S, Shabani AMH, Tamadon F, Rezaei M. Indirect determination of free cyanide in water and industrial waste water by flow injection-atomic absorption spectrometry. Microchim Acta 2007;158:159–63.
[18] Ma J, Dagupta PK. Recent developments in cyanide detection: a review. Anal

Chim Acta 2010;673:117–25.
[19] Boadas-Vaello P, Jover E, Llorens J, Bayona JM. Determination of cyanide and volatile alkylnitriles in whole blood by headspace solid-phase microextraction and gas chromatography with nitrogen phosphorus detection. J Chromatrogr B 2008;870:17–21.
[20] Jung HS, Kwon PS, Lee JW, Kim JI, Hong CS, Kim JW, et al. Coumarin-derived Cu^{2+}-selective fluorescence sensor: synthesis, mechanisms, and applications in living cells. J Am Chem Soc 2009;131:2008–12.
[21] Kim IB, Bunz UHF. Modulating the sensory response of a conjugated polymer by proteins: an agglutination assay for mercury ions in water. J Am Chem Soc 2006;128:2818–9.
[22] Lai CY, Trewyn BG, Jeftinija DM, Jeftinija K, Xu S, Jeftinija S, et al. A mesoporous silica nanosphere-based carrier system with chemically removable CdS nanoparticle caps for stimuli-responsive controlled release of neurotransmitters and drug molecules. J Am Chem Soc 2003;125:4451–9.
[23] Huang CC, Chang HT. Parameters for selective colorimetric sensing of mercury(II) in aqueous solutions using mercaptopropionic acid-modified gold nanoparticles. Chem Commun 2007:1215–7.
[24] Park S, Kim HJ. Highly activated Michael acceptor by an intramolecular hydrogen bond as a fluorescence turn-on probe for cyanide. Chem Commun 2010;46:9197–9.
[25] Xie Y, Ding Y, Li X, Wang C, Hill JP, Ariga K. Selective, sensitive and reversible "turn-on" fluorescent cyanide probes based on 2,2'-dipyridylaminoanthracene-Cu^{2+} ensembles. Chem Commun 2012;48:11513–5.
[26] Xu Z, Pan J, Spring DR, Cui J, Yoon J. Ratiometric fluorescent and colorimetric sensors for Cu^{2+} based on 4,5-disubstituted-1,8-naphthalimide and sensing cyanide via Cu^{2+} displacement approach. Tetrahedron 2010;66:1678–83.
[27] Chen X, Nam SW, Kim GH, Song N, Jeong Y, Shin I, et al. A near-infrared fluorescent sensor for detection of cyanide in aqueous solution and its application for bioimaging. Chem Commun 2010;46:8953–5.
[28] Reddy GU, Das P, Saha S, Baidya M, Ghosh SK, Das A. A CN^- specific *turn-on* phosphorescent probe with probable application for enzymatic assay and as an imaging reagent. Chem Commun 2013;49:255–7.
[29] Jung HS, Han JH, Kim ZH, Kang C, Kim JS. Coumarin-Cu(II) ensemble-based cyanide sensing chemodosimeter. Org Lett 2011;13:5056–9.
[30] Zou Q, Li X, Zhang J, Zhou J, Sun B, Tian H. Unsymmetrical diarylethenes as molecular keypad locks with tunable photochromism and fluorescence *via* Cu^{2+} and CN^- coordinations. Chem Commun 2012;48:2095–7.
[31] Lee JH, Jeong AR, Shin IS, Kim HJ, Hong JI. Fluorescence turn-on sensor for cyanide based on a cobalt(II)–coumarinylsalen complex. Org Lett 2010;12:764–7.
[32] Saha S, Ghosh A, Mahato P, Mishra S, Mishra SK, Suresh E, et al. Specific recognition and sensing of CN^- in sodium cyanide solution. Org Lett 2010;12:3406–9.
[33] Kim S, Noh JY, Park SJ, Na YJ, Hwang IH, Min J, et al. Selective fluorescence assay of aluminum and cyanide ions using chemosensor containing naphthol. RSC Adv 2014;4:18094–9.
[34] Kwon SK, Kou S, Kim HN, Chen X, Hwang H, Nam SW, et al. Sensing cyanide ion via fluorescent change and its application to the microfluidic system. Tetrahedron Lett 2008;49:4102–5.
[35] Xu Z, Chen X, Kim HN, Yoon J. Sensors for the optical detection of cyanide ion. Chem Soc Rev 2010;39:127–37.
[36] Wang F, Wang L, Chen X, Yoon J. Recent progress in the development of fluorometric and colorimetric chemosensors for detection of cyanide ions. Chem Soc Rev 2014;43:4312–24.
[37] Lv X, Liu J, Liu Y, Zhao Y, Chen M, Wang P, et al. Rhodafluor-based chromo- and fluorogenic probe for cyanide anion. Sens Actuators B 2011;158:405–10.
[38] Niu HT, Su D, Jiang X, Yang W, Yin Z, He J, et al. A simple yet highly selective colorimetric sensor for cyanide anion in an aqueous environment. Org Biomol Chem 2008;6:3038–40.
[39] Chen X, Tang R, Jia H, Feng J, Qin J, Li Z. New fluorescent and colorimetric probe for cyanide: direct reactivity, high selectivity, and bioimaging application. ACS Appl Mater Interfaces 2012;4:4387–92.
[40] Chen B, Ding Y, Li X, Zhu W, Hill JP, Ariga K, et al. Steric hindrance-enforced distortion as a general strategy for the design of fluorescence "turn-on" cyanide probes. Chem Commun 2013;49:10136–8.
[41] Lee CH, Yoon HJ, Shim JS, Jang WD. A boradiazaindacene-based turn-on fluorescent probe for cyanide detection in aqueous media. Chem Eur J 2012;18:4513–6.
[42] Cheng X, Zhou Y, Qin J, Li Z. Reaction-based colorimetric cyanide chemosensors: rapid naked-eye detection and high selectivity. ACS Appl Mater Interfaces 2012;4:2133–8.
[43] García F, García JM, García-Acosta B, Martínez-Máñez R, Sancenón F, Soto J. Pyrylium-containing polymers as sensory materials for the colorimetric sensing of cyanide in water. Chem Commun 2005:2790–2.
[44] Li J, Gao J, Xiong WW, Li PZ, Zhang H, Zhao Y, et al. Pyridinium-fused pyridinone: a novel "turn-on" fluorescent chemodosimeter for cyanide. Chem Asian J 2014;9:121–5.
[45] Sun M, Wang S, Yang Q, Fei X, Li Y, Li Y. A new colorimetric fluorescent sensor for ratiometric detection of cyanide in solution, test strips, and in cells. RSC Adv 2014;4:8295–9.
[46] Miyaji H, Kim DS, Chang BY, Park E, Park SM, Ahn KH. Highly cooperative ion-pair recognition of potassium cyanide using a heteroditopic ferrocene-based crown ether–trifluoroacetylcarboxanilide receptor. Chem Commun 2008:753–5.
[47] Li H, Wen Z, Jin L, Kan Y, Yin B. A coumarin-meldrum's acid conjugate based chemodosimetric probe for cyanide. Chem Commun 2012;48:11659–61.
[48] Kim DS, Chung YM, Jun M, Ahn KH. Selective colorimetric sensing of anions in aqueous media through reversible covalent bonding. J Org Chem 2009;74:4849–54.
[49] Shang XS, Li DY, Li NT, Liu PN. A concise synthesis of tunable fluorescent 1,3-dihydroisobenzofuran derivatives as new fluorophores. Dyes Pigment 2015;114:8–17.
[50] Li DY, Shang XS, Chen GR, Liu PN. Solvent-switched benzylic methylene functionalization: addition, ring-opening, cyclization, and unexpected cleavage of C-O and C-C bonds. Org Lett 2013;15:3848–51.
[51] Li DY, Shi KJ, Mao XF, Chen GR, Liu PN. Transition metal-free cascade reactions of alkynols to afford isoquinolin-1(2*H*)-one and dihydroisobenzofuran derivatives. J Org Chem 2014;79:4602–14.
[52] Hu S, Zhang S, Hu Y, Tao Q, Wu A. A new selective pyrazoline-based fluorescent chemosensor for Cu^{2+} in aqueous solution. Dyes Pigment 2013;96:509–15.
[53] Liu Z, He W, Pei M, Zhang G. A fluorescent sensor with a detection level of pM for Cd^{2+} and nM for Cu^{2+} based on different mechanisms. Chem Commun 2015;51:14227–30.
[54] You QH, Lee AWM, Chan WH, Zhu XM, Leung KCF. A coumarin-based fluorescent probe for recognition of Cu^{2+} and fast detection of histidine in hard-totransfect cells by a sensing ensemble approach. Chem Commun 2014;50:6207–10.
[55] Liu Y, Fei Q, Shan H, Cui M, Liu Q, Feng G, et al. A novel fluorescent 'off-on-off' probe for relay recognition of Zn^{2+} and Cu^{2+} derived from *N*,*N*-bis(2-pyridylmethyl)amine. Analyst 2014;139:1868–75.
[56] Huang CB, Li HR, Luo Y, Xu L. A naphthalimide-based bifunctional fluorescent probe for the differential detection of Hg^{2+} and Cu^{2+} in aqueous solution. Dalton Trans 2014;43:8102–8.
[57] Cheng J, Zhang Y, Ma X, Zhou X, Xiang H. Colorimetric and fluorescent pH and Cu^{2+} probes induced by photoisomerization of a maleonitrile-based Salen ligand. Chem Commun 2013;49:11791–3.
[58] Cao M, Jiang L, Hu F, Zhang Y, Yang WC, Liu SH, et al. A dansyl-based fluorescent probe for selectively detecting Cu^{2+} and imaging in living cells. RSC Adv 2015;5:23666–70.
[59] Xie X, Chen X, Li B, Zhang L. Study on a highly selective colorimetric chemosensor for Cu^{2+} detection and its indirect sensing for hypochlorite. Dyes Pigment 2013;98:422–7.
[60] Huang J, Tang M, Liu M, Zhou M, Liu Z, Cao Y, et al. Development of a fast responsive and highly sensitive fluorescent probe for Cu^{2+} ion and imaging in living cells. Dyes Pigment 2014;107:1–8.
[61] Zhou F, Shao J, Yang Y, Zhao J, Guo H, Li X, et al. Molecular rotors as fluorescent viscosity sensors: molecular design, polarity sensitivity, dipole moments changes, screening solvents, and deactivation channel of the excited states. Eur J Org Chem 2011:4773–87.
[62] Shao J, Ji S, Li X, Zhao J, Zhou F, Guo H. Thiophene-inserted aryl–dicyanovinyl compounds: the second generation of fluorescent molecular rotors with significantly redshifted emission and large stokes shift. Eur J Org Chem 2011:6100–9.
[63] Adhikari RM, Neckers DC, Shah BK. Photophysical study of blue, green, and orange-red light-emitting carbazoles. J Org Chem 2009;74:3341–9.
[64] Li X, Kim SH, Son YA. Optical properties of donor-π-(acceptor)$_n$ merocyanine dyes with dicyanovinylindane as acceptor group and triphenylamine as donor unit. Dyes Pigment 2009;82:293–8.
[65] Grabowski ZR, Rotkiewicz K. Structural changes accompanying intramolecular electron transfer: focus on twisted intramolecular charge-transfer states and structures. Chem Rev 2003;103:3899–4032.
[66] Dey J, Warner IM. Dual fluorescence of 9-(N,N-Dimethylamino)anthracene: effect of solvent polarity and viscosity. J Phys Chem A 1997;101:4872–8.
[67] Tang B, Yu F, Li P, Tong L, Duan X, Xie T, et al. A near-infrared neutral pH fluorescent probe for monitoring minor pH changes: imaging in living HepG2 and HL-7702 cells. J Am Chem Soc 2009;131:3016–23.
[68] Li DY, Shi KJ, Mao XF, Zhao ZL, Wu XY, Liu PN. Selective cyclization of alkynols and alkynylamines catalyzed by potassium *tert*-butoxide. Tetrahedron 2014;70:7022–31.
[69] Bader H, Hansen AR, McCarty FJ. Nucleophilic displacements of activated fluorine in aromatic compounds. J Org Chem 1966;31:2319–21.
[70] Li XH, Zheng BH, Ding CH, Hou XL. Enantioselective synthesis of 2,3-disubstituted indanones via Pd-catalyzed intramolecular asymmetric allylic alkylation of ketones. Org Lett 2013;15:6086–9.
[71] Song Y, Jing H, Li B, Bai D. Crown ether complex cation ionic liquids: preparation and applications in organic reactions. Chem Eur J 2011;17:8731–8.
[72] Yang Z, Qin W, Lam JWY, Chen S, Sung HHY, Williams ID, et al. Fluorescent pH sensor constructed from a heteroatomcontaining luminogen with tunable AIE and ICT characteristics. Chem Sci 2013;4:3725–30.
[73] Joshi BP, Park J, Lee WI, Lee KH. Ratiometric and turn-on monitoring for heavy and transition metal ions in aqueous solution with a fluorescent peptide sensor. Talanta 2009;78:903–9.
[74] Benesi HA, Hildebrand JH. A spectrophotometric investigation of the interaction of iodine with aromatic hydrocarbons. J Am Chem Soc 1949;71:2703–7.